Rare by Natural Selection: Disulfide-bonded Supramolecular Antimicrobial Peptides

*Yizhaq Engelberg, Peleg Ragonis-Bachar, and Meytal Landau**

Corresponding author: Meytal Landau - Department of Biology, Technion-Israel Institute of Technology, Haifa 3200003, Israel, and European Molecular Biology Laboratory (EMBL), Hamburg 22607, Germany.

KEYWORDS

Antimicrobials, Fibril, Supramolecular structure, Disulfide, LL-37

ABSTRACT

Human LL-$37_{17\text{-}29}$ is an antimicrobial peptide forming thermostable supramolecular fibrils that surround bacterial cells. The crystal structure of the LL-$37_{17\text{-}29}$ bearing a I24C substitution of most buried position in the fibril, revealed disulfide-bonded dimers that further assembled into a fibrillar structure of densely packed helices. We further demonstrated position-dependent controllable antibacterial activity of LL-$37_{17\text{-}29}$ I24C and other cysteine mutants, mediated by regulation of intermolecular disulfide bonds and their role in the formation of supramolecular

structures. The morphology of the fibrils and their antibacterial mechanism of action might be dependent on their interactions with specific bacteria. The significant effect of disulfide bonds on the assembly into supramolecular structures and their sensitivity to reducing/oxidizing conditions may explain why short helical antimicrobial peptides with single and odd number of cysteines are selected against in nature.

Introduction

Antimicrobial peptides (AMPs), secreted by numerous organisms, are critical for innate immunity, serving antibacterial, antiviral, anti-fungal, anticancer and immunomodulatory roles[1-3]. Host and microbes have evolved several mechanisms to regulate the activity of their own and foreign AMPs, which involve secreted proteases, virulence factors, and other substances[4-7]. For example, in-vivo cleavage of host AMPs can lead to truncated forms with a diverse array of activities and selectivity against microbial strains, alongside additional functions within the immune system[6, 8-16]. Moreover, AMPs activity can be modulated by the formation of well-ordered supramolecular structures[17-23]. One such example is the active core peptide of the human AMP LL-37 (hLL-37_{17-29}), which forms highly stable supra-helical fibrils that interact with bacterial cells[21]. In addition, secretion of reducing and oxidizing factors can regulate the activity of cysteine-containing AMPs that form disulfide bonds essential for their folding and activity[16, 24-35]. For instance, pro-inflammatory processes involve oxidative stress through elevating reactive oxygen species (ROS) concentrations[30-32, 36]. In parallel, some pathogens can promote and express reducing factors that diffuse the oxidative-dependent processes of inflammation and affect the activity of cysteine-rich AMPs[32, 33, 37]. Paradoxically, in the presence of elevated concentrations of

a reduction agent, the antibiotic activity of the human β-defensin 3, which is a cysteine-rich AMP, decreased, while that of β-defensin 1 increased, indicating distinct structure-function relationships and physiological regulation of antimicrobial peptides via reductive pathways[35, 36, 38, 39].

In contrast to the group of cysteine-rich AMPs, which are predominantly β-rich in their secondary structure, and usually form intramolecular disulfide bonds, AMPs with single cysteines can only form intermolecular disulfide contacts, yielding covalently bonded dimers. Since AMPs, especially short amphipathic helices (sahAMPs), tend to self-assemble to enhance antimicrobial activity[21, 40-46], such covalent dimers are expected to affect aggregation, with functional implications. We further expected that an intermolecular disulfide bond dictates the fibrillar morphology of sahAMPs that assemble into functional ordered supramolecular structures, which can be reversed by reducing conditions, thereby regulating activity. To test this hypothesis, we utilized the structural knowledge obtained for hLL-37_{17-29}[21]. We expected, based on the crystal structure, that a cysteine mutant in the most deeply buried position in hLL-37_{17-29} fibril[21] would maintain self-assembly via the formation of an intermolecular disulfide bond, yet with implications on fibril morphology and potentially antibacterial activity. We followingly designed additional seven single-point cysteine mutations in different structural locations in hLL-37_{17-29} and analyzed their antibiotic activity against four bacterial strains, along with their sensitivity to reducing conditions. The findings were correlated to the position of each cysteine along the helical wheel arrangement and within the fibril structure of the native hLL-37_{17-29}. The observations indicated fibril-morphology-dependent activity. This was supported by cysteine substitutions in the amphibian uperin 3.5, another AMP that forms supramolecular structures,

specifically of amyloid fibrils with a functional secondary structure switch between cross-α and cross-β configurations[47].

Overall, this work reinforces the importance of self-assembly in enabling the antibacterial activity of hLL-37_{17-29}, and demonstrates redox-switchable AMP activity, mediated by regulation of intermolecular disulfide bonds and their central role in the formation of supramolecular structures. Owing to their unique effects on AMPs' structure and regulation, we analyzed the prevalence of cysteines compared to other amino acids in AMPs and in proteins in general. We found that single cysteines in sahAMPs are particularly rare.

Experimental Section

Peptides and reagents

hLL-37_{17-29} and uperin 3.5 (UniProt IDs P49913 and P82042, respectively) and their cysteine mutants were purchased from GL Biochem (Shanghai) Ltd. as lyophilized peptides, at >98% purity. Ultra-pure double distilled water (UPddw) and DTT were purchased from Biological Industries.

Bacterial strains and culture media

Micrococcus luteus (*M. luteus*, an environmental isolate) was a kind gift from Prof. Charles Greenblatt from the Hebrew University of Jerusalem, Israel. An inoculum was grown in Luria-Bertani medium (LB), at 30 °C, 220 rpm shaking, 16 h[47]. *Staphylococcus hominis* (subsp. *Hominis Kloos and Schleifer S. hominis*) was purchased from ATCC (ATCC® 27844™). An inoculum was grown in brain-heart infusion medium (BHI), at 37 °C, 220 rpm shaking, 16 h[21]. *Pseudomonas fluorescens* (*P. fluorescens*, subsp. SBW25) was a kind gift from Prof. Roi Kishoni from the Technion, Israel. An inoculum was grown in LB, at 28 °C, with 220 rpm shaking, for 16

h[48, 49]. *Escherichia coli*, subsp. *k3 3106* (*E. coli*) was a kind gift from Prof. Ehud Gazit from Tel Aviv University, Israel. An inoculum was grown in LB, at 37 °C, with 220 rpm shaking, for 16 h.

Dynamic light scattering (DLS)

The particles size distribution of hLL-37_{17-29} and its cysteine mutants, Q22C and I24C, with or without DTT, was compared using DLS. Lyophilized peptides were dissolved in UPddw to a concentration of 1 mM. DTT powder was freshly dissolved in UPddw to a concentration of 1M and was added to relevant peptides samples to a final concentration of 10mM. After a short vortex, the samples were incubated for 24 h, at 25 °C. Samples (20-30 µl) were then mounted using 1.0x1.0 mm disposable cuvette capillaries with a thickness of 200 µm (Malvern, ZSU0003), which were then sealed with clay. Capillaries were placed within low-volume disposable sizing cell Kitholder (Malvern, ZSU1002). Light scattering readings were collected using ZetaSizer Ultra (Ultra ZS; Malvern). The hydrodynamic radii (Rh) were determined using a back-scattered light at a fixed angle of 90°. A 633 nm wavelength He-Ne laser was used. The cell holder was maintained at 25°C for the measurement. Scattering data were collected from at least three different measurements with at least five sequential scans for each measurement. The mean of the volume intensities was sub-categorized into three cumulative subpopulations (S.P) of sizes: 0.3-30 nm, 30-3000 nm and above 3000 nm (>3000 nm), to yield a cumulative volume of particles within the sample. The average size of the total particles in each sample, and particularly in each subcategory, was determined by summing the score of the mean average volume intensities their correlative sizes within each range, as described elsewhere[21]. Error (E) was calculated by dividing the standard deviation at the square of the measurements number. Error bars indicate the cumulative error for each subpopulation and were calculated by squaring the sum of the squares of the error values in the subpopulation range.

Transmission electron microscopy (TEM)

To image the peptides in the presence of bacterial cells, *M. luteus* and *S. hominis* were grown for 24 h in LB, approximately 1.5×10^9 bacteria cells were washed three times by pelleting the bacteria suspension via centrifuging at 2000xg and replace the supernatant with 10 mM potassium phosphate buffer, pH = 7.4. Lyophilized peptides were dissolved in the same buffer and added to the bacterial pellets, which were re-suspended to the final peptide concentrations (as detailed in the figures). DTT was freshly dissolved in UPddw to a stock solution of 1 M, which was further dissolved in the same buffer as the peptides to a concentration of 100 mM. DTT was applied to relevant peptides in x5-20 molar ratio excess relative to the peptide (specific ratios are indicated in the relevant figures). Samples were then incubated at 30 °C or at 37 °C, with 220 rpm shaking, for 2 h. TEM grid preparation and visualization were performed as follows: samples (4–5 µl) were applied directly onto glow-discharged (easiGlow; Pelco, Clovis, CA, USA, 15 mA current; negative charge; 25 s time) 400 mesh copper grids, with a grid hole size of 42 µm, stabilized with Formvar/carbon (Ted Pella, Inc.), and allowed to adhere for 45 s. Samples were than stained with 1% uranyl acetate solution (Electron Microscopy Science, 22400-1) for 30 s before being blotted with Whatman filter paper. Specimens were examined with a FEI Tecnai T12 G2 electron microscope, at an accelerating voltage of 120 kV, or a FEI Tecnai G2 T20 electron microscope, at an accelerating voltage of 200 kV.

Bacterial growth studies

Determination of minimal inhibitory concentrations (MIC): *M. luteus* and *S. hominis* inocula were diluted to OD_{600} = 0.1. $hLL\text{-}37_{17\text{-}29}$, uperin 3.5 and cysteine mutants were dissolved in phosphate buffered saline (PBS) buffer into peptides stocks solutions. Peptides stocks solutions were then diluted in the bacteria medium. Control and blank samples contained everything but

peptides or everything but bacteria, respectively. Experiments were performed in a sterile 96-well plate, with a final reaction volume of 100 µl. Bacterial growth (OD_{600}) was measured by a plate reader (FLUOstar omega or CLARIOstar, BMG LABTECH), during a 24 h incubation, at different temperatures (as described previously), with 220 rpm shaking. Blanks were subtracted and the ratio of the test samples versus their respective controls (everything but the peptide) were calculated. MIC values were defined as the minimal concentration of the peptide which yielded less than 20% of the OD_{600} ratios. All experiments were performed in triplicates and were averaged. The entire experiment was repeated at least three times on different days, and the mean was calculated from the averaged triplicates of all biological repeats. Error bars represent standard errors of the mean.

DTT sensitivity experiments: DTT was freshly dissolved in UPddw to a stock with a concentration of 1 M, and diluted in PBS to working stocks of 200-300 mM. Stocks of peptides were initially dissolved in PBS and then DTT was added to a final concentration of x10 molar ratio compared to the peptide concentration (the specific concentrations are indicated in the relevant figures). In studies of dose response effect of DTT on bacteriostatic activity of peptides, peptides were diluted into a fixed concentration of 50 µM and DTT was added with three molar ratios of x2, x 10 and x20, comparing to the peptides concentrations. Samples with DTT were compared to their relevant controls which contained everything but the peptides (and the same DTT concentrations). All experiments including controls and blanks, were tested in triplicates on at least three different days. Measurements were averaged. Appropriate blanks were subtracted, and the mean values were plotted against peptide concentration. Standard errors of the mean of OD_{600} readings are presented as error bars.

Crystallization conditions

I24C lyophilized peptide and DTT were both dissolved in UPddw to 10 mM (~17 mg/ml) and 100 mM, respectively. DTT was added to the peptide solution to a final concentration of 0.1 mM. Samples were vortexed and centrifuged (14,000 rpm, 4˚C, 10 min). Crystals of I24C with DTT were grown, at 20°C, from a reservoir solution containing 2.8 M sodium acetate trihydrate, pH 7.0. (Hampton Research, HR2-134 (Index HT), well B12), using the hanging-drop vapor diffusion technique. Crystals were flash-frozen in liquid nitrogen before X-ray data collection.

Structure determination and refinement

X-ray diffractions of I24C were collected at the EMBL micro-focused beam at the high brilliance 3rd Generation Synchrotron Radiation Source at DESY: PETRA III, Hamburg, Germany. The wavelength of data collection was 0.976Å. Data indexing, integration, and scaling were performed using XDS and XSCALE[50]. Phases were obtained by molecular replacement using Phaser[51]. Molecular replacement of I24C phases was performed using the atomic structure of $gLL37_{17\text{-}29}$ coordinates (PDB 6S6N) as a search model. Crystallographic refinements were performed with Refmac5 [52]. Model building was also performed using Coot[53] and illustrated with Chimera[54]. The structure of I24C was determined at 1.5 Å. There were two peptide chains in the asymmetric unit and 16 water molecules. No residues were detected in the disallowed region at the Ramachandran plot. Crystallographic statistics are presented in Table S1.

Calculations of structural properties

The electrostatic potential map and hydrophobicity coloring presented in the figures were generated using Chimera[54]. The values of the hydrophobicity scale were according to Kyte and Doolittle[55]. The electrostatic potential was calculated using APBS-PDB2PQR[56]. Helix

amphipathicity, and chemical and physical properties of sequences were calculated with HeliQuest[57]. The helical wheels were also generated by HeliQuest[57].

Solvent-accessible surface area calculations

Solvent-accessible surface areas (SASAs) were calculated using AREAIMOL, with a probe radius of 1.4Å[58, 59], via the CCP4 package[52]. The solvent-accessible buried surface area of each chain in the asymmetric unit was calculated as the area difference between the isolated chain and the chain within the fibril assembly, and is presented as the percentage of the total SASA of the chain. The SASA per residue within different isolated helical assemblies is presented in Table S2.

Statistical analysis of amino-acid frequencies

Databases and protein groups analyzed

To calculate amino acid frequency in different protein groups, we used the Swiss-Prot database of curated proteins[60], and the ($CAMP_{R3}$) database[61] for a collection of anti-microbial peptides. All 20 amino acid frequencies were calculated in four different protein groups: proteins from the Swiss-Prot database[60] (n=563972 protein sequences (PG1)), proteins shorter than 40 amino acids from the Swiss-Prot database (n=9526 sequences (PG2)), AMPs with a validated activity shorter than 100 amino acids from the $CAMP_{R3}$ database[61] (n=2300 sequences (PG3)), and AMPs with a validated activity shorter than 40 amino acids from the $CAMP_{R3}$ database[61] (n=1808 sequences (PG4)). For each group, the frequency of each amino acid was calculated as follows:

$$frequency\ of\ amino\ acid\ X \in PG = \frac{\sum_{p \in PG} number\ of\ amino\ acid\ X \in p}{\sum_{p \in PG} length\ of\ p}$$

where PG# denotes the four different protein groups and P for protein.

Secondary structure prediction and amphipathicity

The Jpred webserver[62] was used to predict secondary structures of each peptide in the databases. Jpred relies on the A Neural Network Protein Secondary Structure Prediction Method (JNet algorithm), one of the most accurate methods for secondary structure prediction[62]. To adapt the data to Jpred input requirements, amidation of Ctr or Ntr were removed (if existed) and peptides smaller than 20 amino acids were duplicated $\lfloor \frac{20}{peptide\,length} \rfloor$ times to obtain a minimum length of 20 amino acids. We defined the secondary structure as helical using three threshold values: (1) minimal number of residues predicted as helix is eight, or the residues predicted as helix encompass at least 80% of the sequence length (2) Minimal gap of four residues between segments predicted as helix and (3) Minimal Jpred predicted score of the helix is at least two, on average, over the predicted residues encompassing the helix (this is considered a low threshold, over a range of probability scores going up to nine). Thus, we were permissive in defining helical sequences. The hydrophobic moment (μ H) was calculated as $\frac{1}{N}\sqrt{\left[\sum_{n-1}^{N} H_n \sin(n\delta)\right]^2 + \left[\sum_{n-1}^{N} H_n(\cos(n\delta))\right]^2}$, where N is the sequence length, H_n is the hydrophobicity of the nth amino acid in the sequence according to its octanol\water partition[63] and $n\delta$ is the angle separating side chains along the backbone, with $\delta = 100°$ for an α -helix[64]. The μ H threshold was determined as the mean μ H calculated for all AMPs shorter than 40 amino acids that were predicted as helical, and helical sequences were defined as amphipathic in case the calculated μ H was higher than the μ H threshold.

Specific amino acid frequency calculations in sahAMPs

The number of experimental validated of AMP sequences containing a single cysteine was counted among AMPs shorter than 40 amino acids from the $CAMP_{R3}$ database[61], among short

AMPs predicted as helical, and among those also defined as amphipathic. The numbers are presented in Table S6. As controls, the numbers of sequences from the same groups having a single tyrosine, due to its similar helical propensity, according to the Cho-Fasman table65 and of arginine, due to its similar frequency in sahAMPs as cysteine, were counted. To graphically present the number of AMPs containing single cysteine, tyrosine, or arginine residues (residue 'X'), normalized to their frequencies in AMPs shorter than 40 amino acids from the $CAMP_{R3}$ database[61], including 1808 sequences (PG4), we used :

$$\frac{Number\ of\ AMPs\ containing\ a\ single\ residue\ 'X'}{'X'\ frequency \in AMPs\ shorter\ than\ 40\ residues \cdot Number\ of\ AMPs\ horter\ than\ 40\ residues} \cdot 100$$

Results

The hLL-37_{17-29} I24C mutant forms supra-helical fibrils with inter-molecular disulfide bonds

In a recent characterization of the atomic details of stable supra-helical hLL-37_{17-29} fibrils[21], we report on fibrils composed of a basic unit of four-helix bundles with a hydrophobic core, with Ile24 located at the center of the bundle, completely buried within this assembly[21]. Substituting this position with alanine (I24A), which is less bulky and hydrophobic, or with various polar residues, fully abolished the ability of hLL-37_{17-29} to inhibit the growth of *Micrococcus luteus* (*M. luteus)*, as well as its ability to form ordered supramolecular structures[21] . We nevertheless hypothesized that a substitution to cysteine will maintain inter-molecular associations via the formation of a stabilizing disulfide bond in the center of the hydrophobic face of the hLL-37_{17-29} amphipathic helix.

Solving the crystal structure of the hLL-37_{17-29} I24C mutant at 1.5Å resolution (PDB code 7NPQ, Table S1), revealed a fibrillar structure of densely packed helices (Figures 1&2 and

Figure S1). The asymmetric unit contained two chains of amphipathic helices covalently connected via a disulfide bond between Cys24, with the hydrophobic sides facing each other (Figure 1 and Figure S2). The dimers were further assembled into a tightly packed structure of a protofibril encapsulating the hydrophobic core, with a different fibrillar assembly compared to the native hLL-$37_{17\text{-}29}$, yet also displaying densely packed helices[21] (Figures S1-S2). While the four helix-bundles of hLL-$37_{17\text{-}29}$ and the dimers of the I24C mutant showed a different orientation of helices, in both the hydrophobic face comprised a large portion of the inter-helical interface (Figure S2 and Table S2).

In hLL-$37_{17\text{-}29}$ I24C, only a mean 17% of the solvent-accessible surface areas of individual helices, was buried within the dimer, yet 65% of the solvent-accessible surface area of chain A, and 78% of that of the chain B, was buried within the general assembly, indicating overall compact fibrillar packing. In comparison, in the fibrillar structure of the native hLL-$37_{17\text{-}29}$, on average, 67% of the solvent-accessible helix surface area was buried within the assembly[21], showing similar compactness compared to the structure of hLL-$37_{17\text{-}29}$ I24C (Table S2). Both hLL-$37_{17\text{-}29}$ and the I24C mutant structures displayed much tighter packing compared to the crystal structure of full-length LL-37, in which only 45% of the helix buried within the protein assembly was composed of associated dimers (for PDB ID 5NNT)[66].

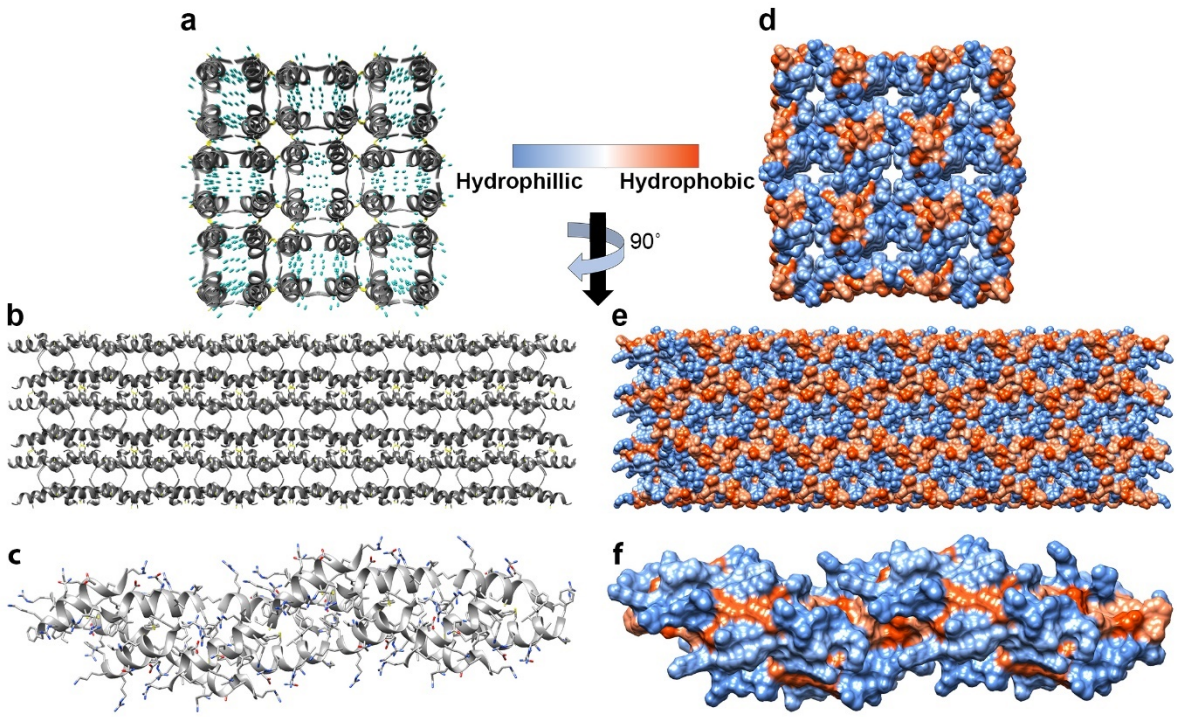

Figure 1. Fibrillar crystal atomic structure of the hLL-37$_{17-29}$ I24C mutant, determined at 1.5 Å resolution (PDB code 7NPQ, Table S1), (a-c) The hLL-37$_{17-29}$ I24C helices are presented as gray ribbons. Cysteine residues are shown as sticks and colored by atom type, with sulfur in yellow. In panel c, side chains are shown as sticks and colored by atom type, with nitrogen in blue and oxygen in red. (d-f) The same orientations as in panels a-c, respectively, displayed in a surface representation colored by hydrophobicity, according to the scale bar. (a&d) Top view down the fibril axis. Water molecules are presented as cyan balls in panel a. (b&e) The orientation is rotated by 90˚ relative to panels a&d, for a view along the fibril axis. (c&f) An isolated helical assembly of an elongated protofibril.

The four helix-bundles of the native hLL-37$_{17-29}$ further assembles via polar interactions and a small hydrophobic patch[21]. Similarly, in the I24C structure, covalent dimers further assembled via a network of interactions (Figure S3), including putative salt bridges between Asp26 on chain

A in one dimer and Lys18 on chain B of an adjacent dimer, and between Asp26 on chain B and Arg29 of chain A of an adjacent helix. In addition, the carboxyl group of the C terminus of chain A formed putative salt bridges with the side chain of Arg23 of chain A of another dimer and with the side chain of Arg29 from chain B of a third dimer. The carboxyl group of the C terminus of chain B formed putative salt bridges with the side chain of Arg23 of chain B of a fourth dimer. Overall, each dimer was involved in 10 putative salt bridges with five surrounding dimers. The fibrillar assembly was further stabilized by Π-stacking and cation-Π interactions between two Phe17 residues from different dimers and two Arg23 residues from both chains of a third dimer (Figure 2). Moreover, an elongated hydrophobic core extended along the fibril. The top-view into the fibril axis depicts the hydrophobic core, tightly packed and completely deficient of water molecules (Figure 1 and Figure S1). The side-view of the fibril depicts the helical assembly encapsulating the hydrophobic core into an elongated protofibril. The packing between these elongated protofibrils is mostly polar, mediated by water molecules and polar interactions (Figure 1 and Figures S1&S3).

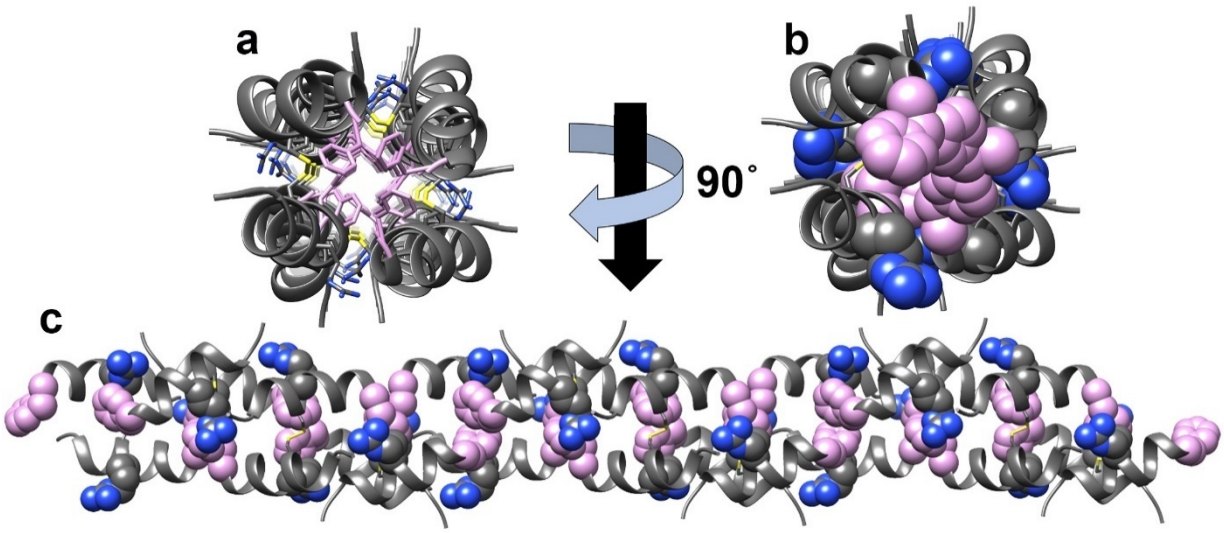

Figure 2. Disulfide-bound helical dimers of the hLL-37_{17-29} I24C mutant further assemble into a fibril via a network of cation-Π and hydrophobic interactions. The hLL37_{17-29} I24C protofibril is shown in a grey ribbon representation. (a-b) A view down the fibril axis. (c) A side-view along the fibril axis of the protofibril, rotated 90˚ compared to panels a-b. Phe17 side chains are colored pink, and Arg23 and Cys24 side chains are colored by atom type (nitrogen in blue and sulfur in yellow). Phe17 and Arg23 are presented as sticks (a) or as space-filled atoms (b&c). Cys24 is presented as sticks in all panels.

The electrostatic potential map of the of hLL37_{17-29} I24C covalent dimer, the basic self-assembling unit of the fibril, showed a positively charged surface (Figure S4), similar to the hLL-37_{17-29} structure, which has arginine residues lining the surface of the four-helix bundles[21]. Overall, despite the different general assembly, hLL-37_{17-29} and the I24C mutant both displayed a fibrillar structure with a surface composed of zigzagged hydrophobic and positively charged belts, which likely indicate interactions with and subsequent disruption of negatively charged lipid bilayers, such as bacterial membranes. The I24C mutant indeed showed similar minimal inhibitory concentration (MIC) against *Micrococcus luteus* (*M. luteus*) as hLL-37_{17-29} (Table 1). Nevertheless, a reducing agent, dithiothreitol (DTT), abolished this bacteriostatic activity (Figure S5), indicating the functional significance of disulfide-mediated intermolecular assemblies.

Formation and reduction of disulfide bonds in hLL-37_{17-29} cysteine mutants affect bacteriostatic activity and selectivity

The potential contribution of intermolecular disulfide bond formation to antibiotic activity and selectively was further assessed using I24C and additional seven single-point cysteine mutations in different locations along the helical wheel of the amphipathic hLL-37_{17-29} (Table 1, Figure 3,

and Table S3). Bacteriostatic activity was tested against four bacterial species including Gram-positive *M. luteus*, *Staphylococcus hominis* (*S. hominis*), and Gram-negative *Escherichia coli* (*E. coli*) and *Pseudomonas fluorescens* (*P. fluorescens*). The effect of reducing conditions was examined by measuring growth inhibition with and without DTT at three different concentrations of the mutant peptides around their MIC levels (Figure 3 and Figures S5-S8). For all bacterial species tested, the effect of DTT on bacteriostatic activity, if present, was observed below and around the MIC concentrations of the peptides, while it was mostly ineffective at above-MIC concentrations (Figures S5-S8). The effect of DTT on peptide activity is dose-dependent, as shown for example for the activity of F27C against *E. coli* (Figure S9).

hLL-37_{17-29} I24C was the least active mutant, with bacteriostatic activity observed only against *M. luteus* (Table 1), highlighting its critical location in the center of the helix and the most buried residue in the hLL-37_{17-29} fibril. The observed inactivity of I24C against three bacterial species corresponds to the effect of substitutions in this positions to alanine or various polar residues, which fully abolished the activity of hLL-37_{17-29} against *M. luteus* and the formation of ordered fibrils[21] . The I24C substitution leads to a formation of an altered fibril packing and morphology, which might be incompatible with toxic activity against bacterial species less sensitive than *M. luteus*. Moreover, the addition of DTT abolished I24C activity against M. luteus (Figure 3), further indicating the dependency on the formation of specific supramolecular structures.

Table 1. Bacteriostatic activity of hLL-37_{17-29} mutants against four bacterial strains

MIC values (μM)				
	M. luteus	***S. hominis***	***E. coli***	***P. fluorescens***
hLL-37_{17-29}	25±2	39±1	47±3	136±4

F17C	22±2	64±6	63±5	164±5
K18C	16±3	50±8	100±7	>200
I20C	22±2	150±10	75±3	>200
V21C	17±3	43±7	30±0	113±5
Q22C	12±4	48±8	40±0	166±5
I24C	22±4	>200	>200	>200
F27C	13±3	28±5	37±3	151±3
L28C	20±0	37±3	43±3	75±3

Growth inhibition of four bacterial species by hLL-37_{17-29} and hLL-37_{17-29} single-point cysteine mutants, indicated by MIC values in μM, tested up to 200 μM. The experiments were performed at least four times, on different days. Error values of MIC values indicate the standard error of all repeat measurements.

Cysteine mutants in other positions than Ile24 showed high sensitivity to DTT, which abolished activity of all active mutants against *S. hominis*, except for that bearing the K18C substitution, and that of all active mutants against *E. coli*, except of the F17C and Q22C mutants (Figures S6-S7). *P. fluorescens* was relatively resistant to all hLL-37_{17-29} peptides, which were either non-active or showed higher MICs compared to other bacteria strains (Figure S8). However, in contrast to other bacterial species, *P. fluorescens* showed sensitivity to DTT itself (Figure S10). The effect of DTT on the activity of the hLL-37_{17-29} peptide variants with high MIC values against *P. fluorescens* thus could not be determined without considerable error resulting from the toxic effect of DTT alone. From what we could still determine, namely for the more active mutants F17A, V21C, and L28C, DTT abolished their activity against *P. fluorescens* (Figure 3 and Figure S8). Overall, DTT had a significant negative effect on hLL-37_{17-29} mutants' activity, around their MIC levels, against three bacterial species.

	DTT sensitivity			
	M. luteus	*S. hominis*	*E. coli*	*P. fluorescens*
hLL-37 $_{17-29}$	-	-	-	-
F17C	-	+	+	+
K18C	-	-	+	o
I20C	-	+	+	o
V21C	-	+	+	+
Q22C	-	+	-	N/A
I24C	+	o	o	o
F27C	-	+	+	N/A
L28C	-	+	+	+

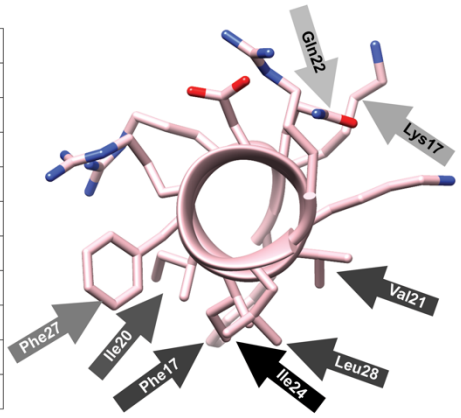

Figure 3. DTT sensitivity of hLL-37$_{17-29}$ with single-point cysteine mutants. The ability of DTT to alternate the growth inhibition of four bacterial species, at x10 molar ratio, is indicated by (+) or (-), as detailed in Figures S5-S8. In cases of non-bacteriostatic peptides, sensitivity to DTT was not relevant and the effect is marked with (o). Cases in which the DTT was too toxic for the bacteria at the indicated concentrations are marked by N/A. Mutant sensitivity to DTT was manually scaled (according to the percentage of times DTT showed an effect on an active mutant) and is indicated is the left column using a gray color scale, with light to dark shades indicate low to high DTT sensitivity, respectively. On the right panel, arrows with the same gray coloring scheme indicate the specific residue on a single hLL37$_{17-29}$ helix, as determined by the crystal structure. Non-carbon atoms are colored by atom type (oxygen in red and nitrogen in blue).

DTT induces smaller particle sizes of the I24C mutant, but not of native hLL-37$_{17-29}$ or the Q22C mutant

The effect of DTT on self-assembly was evaluated by assessing the particle size distribution of the peptides using dynamic light scattering (DLS) (Figure 4 and Table S4). The particle size population of native hLL-37$_{17-29}$ indicated large assemblies, with an average diameter of few hundreds to thousands of nanometers, with or without DTT. In contrast, hLL-37$_{17-29}$ I24C

displayed a drastic DTT dependent reduction in particle sizes. Specifically, the untreated hLL-$37_{17\text{-}29}$ I24C samples contained ~34% small particles, with an average diameter of 1.4 nm which roughly corresponds to a small oligomer of few subunits, with the remainder forming large particles of few hundreds to thousands of nanometers, with an average diameter of 622 nm. With the addition of DTT, 100% of the hLL-$37_{17\text{-}29}$ I24C particles were small with an average diameter of 1.3 nm. This indicates that self-assembly of I24C is very much dependent on disulfide bond formation, and can be reversed by a reducing agent. For comparison, we examined particle size distribution of the hLL-$37_{17\text{-}29}$ Q22C mutant that was the least sensitive to the effect of DTT on bacteriostatic activity (Figure 3). The addition of DTT had no effect on the Q22C large particles distribution and no significant effect on the average diameter of the overall particles in the solution, similar to the native hLL-$37_{17\text{-}29}$. This suggest that a disulfide bond is either not involved, or not critical for self-assembly of the hLL-$37_{17\text{-}29}$ Q22C mutant. The correspondence between disulfide-independent self-assembly to the low sensitivity to DTT of bacteriostatic activity further supports the significance of supramolecular species to function.

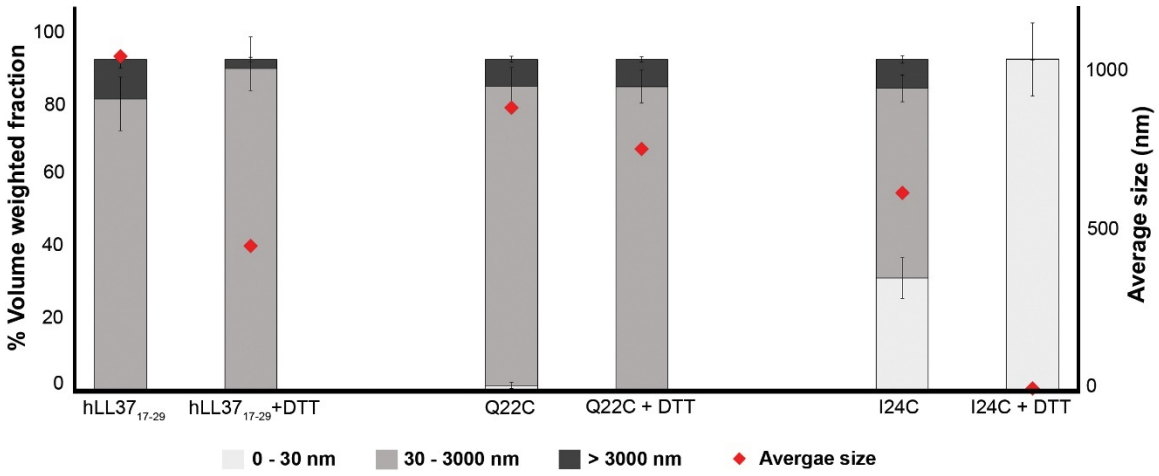

Figure 4. Particle volume-weighted size distribution of sub-populations of hLL$37_{17\text{-}29}$ and its Q22C and I24C mutants as measured by dynamic light scattering (DLS). Three sub-populations

of particle sizes are colored in different shades. The average size of the total particles population in each sample is presented by red rhombuses. The values presented here and the average size of the particles in each subpopulation and of the total population, are specified in Table S4. Statistical evaluations are described in the Experimental section.

Visualization of self-assembly in the presence of bacterial cells

Considering that cell membranes might affect aggregation and fibril morphology, the possible correlation between self-assembly of inter-molecular disulfide bonds to the antibiotic activity of hLL-$37_{17\text{-}29}$ cysteine mutants was evaluated by electron microscopy, imaging the structures formed on the cells of *M. luteus* and *S. hominis*. The active I24C mutant formed clustered structures on the membranes of *M. luteus*, while the addition of DTT led to amorphous aggregation around the bacterial membrane (Figure 5b&e), corresponding with its negative effect on bacteriostatic activity (Figure 3). Comparably, I24C, which was inactive against *S. hominis*, showed no observable formation of ordered structures around its cells, with or without DTT (Figure 6b&e). The F27C mutant, whose activity against *M. luteus* was not affected by the addition of DTT, formed dense aggregations on the bacterial membranes, while the addition of DTT resulted in the formation of even more defined fibril structures (Figure 5c&f). The Q22C mutant was active against all bacterial species, and its activity was affected by the addition of DTT only against *S. hominis* (Figure 3). Q22C formed immense amorphous structures around *S. hominis* cells, while the addition of DTT led to formation of flake-like structures (Figure 6c&f). This indicates that in the presence of *S. hominis*, Q22C is aggregating with and without DTT, in correspondence to the DLS results (Figure 4 and Table S4), but the morphology is affected by the addition of DTT (Figure 6).

Overall, the level of bacteriostatic activity appeared to be correlated with changes in the morphology of the aggregates and fibrils of hLL-37_{17-29} mutants. This is reminiscent of amyloid oligomer and fibril polymorphisms that dictates level of toxicity[67-69]. The morphological changes of the aggregates also seemed correlated with presence of DTT. Depending on the position of the cysteine residue along the helical wheel, the inter-molecular disulfide bonds may play a role in rearranging or supporting, but not necessarily in forming, of the supra-helical assembly. This was previously suggested for the assembly of a transmembrane helix bundle[38]. As mentioned, the reduction in mutant activity against the different bacteria by the addition of DTT was observed only below and around MIC values, while DTT was basically ineffective at high peptide concertation (Figures S5-S8). This suggests that at high concentrations, peptide self-assembly of all mutants is independent on the formation of a disulfide bond.

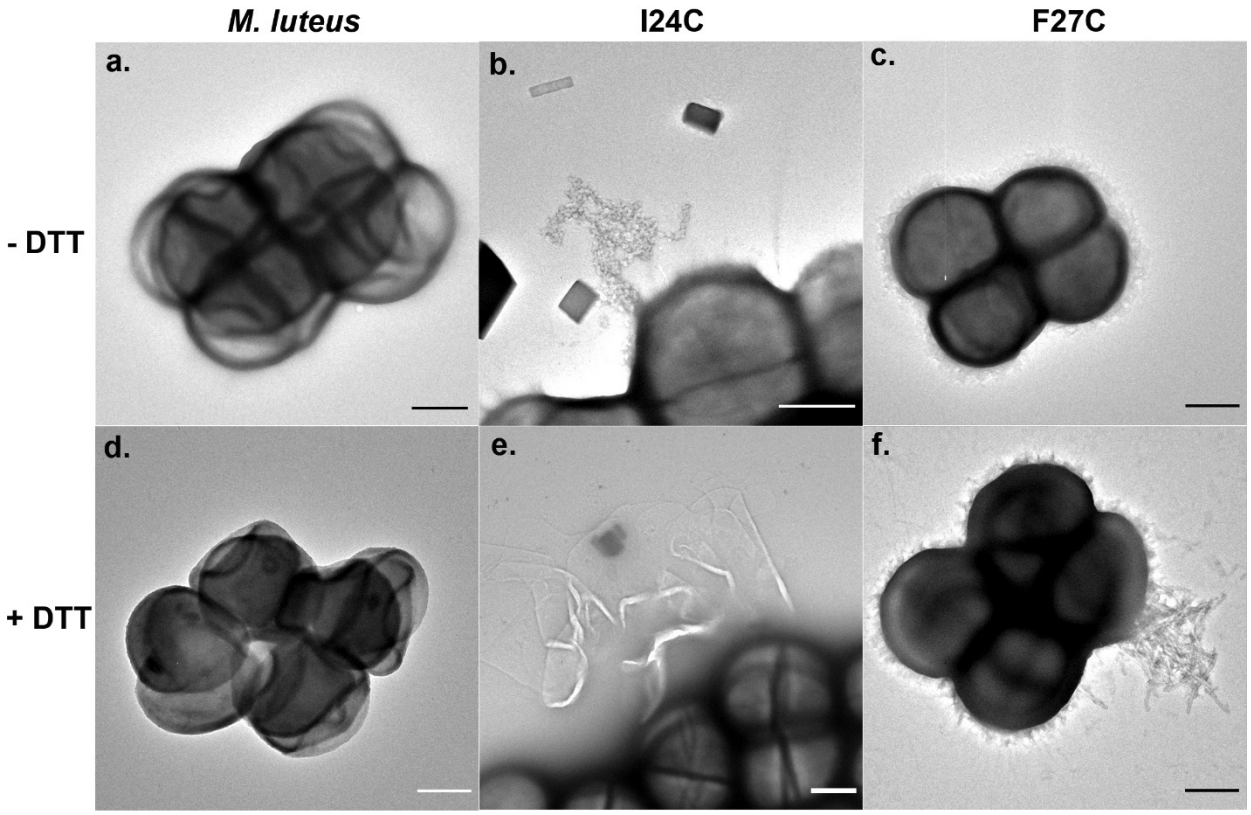

Figure 5. Self-assembly of the hLL-$37_{17\text{-}29}$ I24C and F27C mutants around *M. luteus* cells with and without DTT. Electron micrographs of *M. luteus* incubated alone or with 1 mM DTT (a&d), and with the addition of the hLL-$37_{17\text{-}29}$ I24C (b&e) or hLL-$37_{17\text{-}29}$ F27C (c&f) mutants added at above-MIC concentrations of 40 µM and 50 µM, respectively. The peptides and bacteria were incubated for 4 h without (b-c) or with (e-f) DTT at x12.5 or x17 molar ratio compared to the concentrations of I24C and F27C, respectively. Scale bars represent 500 nm.

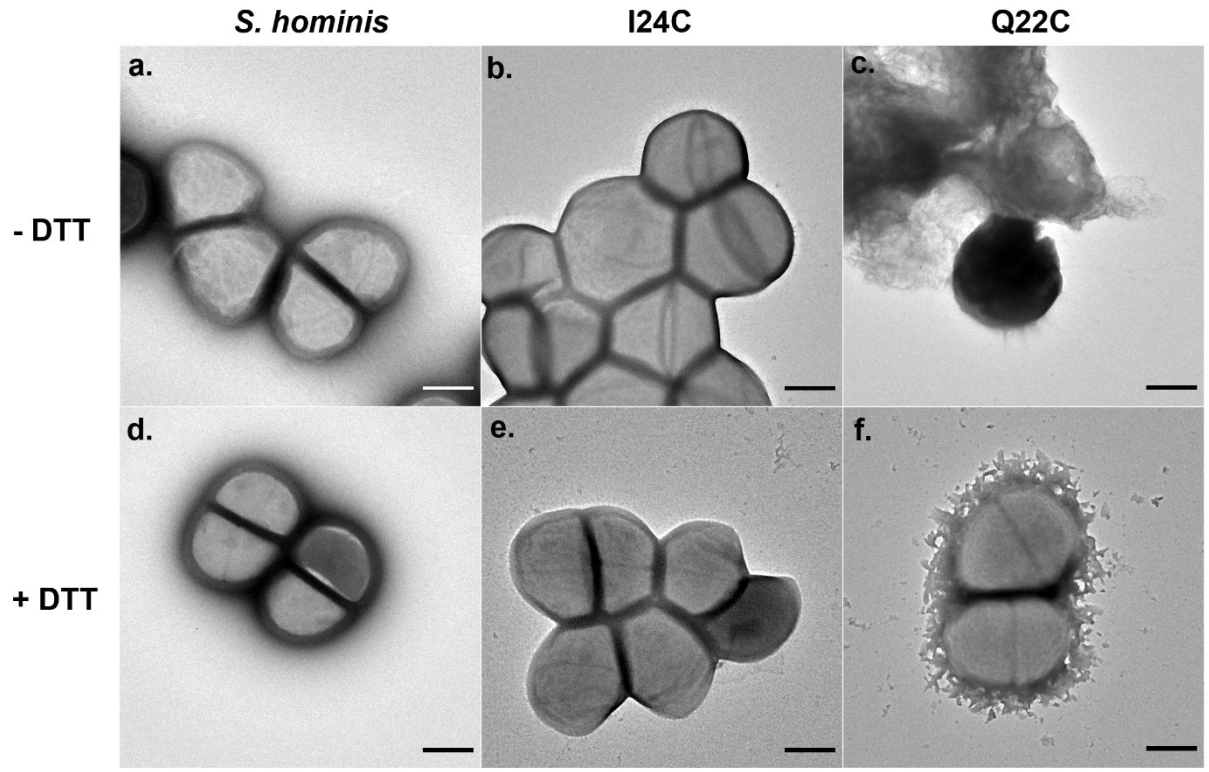

Figure 6. Self-assembly of the hLL-$37_{17\text{-}29}$ I24C and Q22C mutants around *S. hominis* cells with or without DTT. Electron micrographs of *S. hominis* incubated alone (a), with 1 mM DTT (d), or with the hLL-$37_{17\text{-}29}$ I24C (b&e) or hLL-$37_{17\text{-}29}$ Q22C (c&f) mutants, added at concentrations of 150 µM and 60 µM, respectively. The peptides and bacteria were incubated for 4 h without (b-c) or with (e-f) DTT at x7 or x17 molar ratio compared to the concentrations of I24C and Q22C, respectively. Scale bars represent 500 nm.

DTT affects bacteriostatic activity of the amphibian sahAMP uperin 3.5

To assess the generality of DTT sensitivity of sahAMPs cysteines mutants, we designed mutations in uperin 3.5, a sahAMP secreted on the skin of Australian toadlets. Uperin 3.5 was recently shown to form amyloid cross-α fibril structures of tightly mated helical sheets, formed via helices stacked perpendicular to the fibril axis[47]. The cross-α configuration was initially observed in the cytotoxic bacterial PSMα3[70], which shows similar sequence attributes to hLL-$37_{17\text{-}29}$, along with the shared ability to form fibrils composed of densely packed helices[21]. We designed uperin 3.5 with one of two cysteine mutations, I13C and S11C (Table S5a), located at the center of the hydrophobic and polar faces of the helix, respectively. Both the native uperin 3.5, and its I13C and S11C mutants, were active against *M. luteus*, with MICs of 5-7 μM (Table S5b). While DTT had no effect on the activity of native uperin 3.5, it reduced the activity of both mutants around their MIC levels (Figure S11 and Table S5b), with a greater impact on the I13C mutant, located on the hydrophobic face, as compared to the S11C mutant, located on the hydrophilic face. This is likely due to more efficient supramolecular fibrillar structure formation when the disulfide bond strengthens the hydrophobic intermolecular interfaces.

sahAMPs with single and an odd number of cysteines are rare

Our findings showed that reduction of disulfide bonds can affect bacteriostatic activity of hLL-$37_{17\text{-}29}$ and uperin 3.5, putatively via modulating the formation and morphology of supramolecular structures. We sought to determine the abundance, among the thousands of experimentally validated AMPs included in the $CAMP_{R3}$ database[61], sahAMP (<40 amino acids) which contain a single or odd number of cysteine residues, rendering them more likely to form dimers connected via intermolecular disulfide bonds. AMPs were defined helical according to a

secondary structure prediction performed by the Jpred server[62] . AMPs were defined as amphipathic if the hydrophobic moment (μ H) of the helical part of the sequence was above the average μ H for all short helical AMPs.

Despite the relatively high abundance of cysteine residues in AMPs, compared to proteins in general (Figure 7), the prevalence of sahAMPs with a single cysteine was especially low (Figure 8 and Table S6). Specifically, we found that among 553 sahAMPs with experimentally validated antimicrobial activity, only 7 contained a single cysteine (Table S7). In comparison, the prevalence of sahAMPs with a single tyrosine, a residue which shows similar secondary structure propensities to cysteine[71], was significantly higher (38 sequences), despite the lower abundance of tyrosine residues in short AMPs (Figure 7&8 & Table S6). The high number (81 sequences) of sahAMPs with a single arginine, a residue which shows similar abundance in short AMPs to cysteine, again emphasizes the strong selection against sahAMPs with a single cysteine. Expending the search to AMPs containing an odd number of cysteine, tyrosine or arginine residues revealed the same trend (Table S6).

	SP	SP < 40aa	AMPs < 100aa	AMPs < 40aa
A	8	7	8	8
R	5	6	6	6
N	4	4	4	3
D	5	3	3	2
C	2	4	7	6
Q	4	3	3	2
E	7	4	3	2
G	7	8	11	11
H	2	2	2	2
I	6	7	6	7
L	10	9	9	11
K	6	7	10	11
M	2	3	1	1
F	4	5	4	5
P	5	5	5	4
S	7	6	6	6

T	6	5	4	4
W	1	1	2	2
Y	3	3	2	2
V	7	7	6	6

Figure 7. Amino acid prevalence in AMPs and proteins in general. The figure outlines amino acid frequencies in four groups: proteins from the Swiss-Prot (SP) database[60] (n=563972), proteins shorter than 40 amino acids (aa) from the Swiss-Prot database (n=9526), experimentally validated AMPs shorter than 100 amino acids from the $CAMP_{R3}$ database[61] (n= 2300), and AMPs shorter than 40 amino acids from the $CAMP_{R3}$ database[61] (n= 1808). The amino acid frequencies are presented as percentage (%), indicating relative abundance. The color code ranges from lowest to highest prevalence, colored in increasingly deep shades of blue to red, respectively.

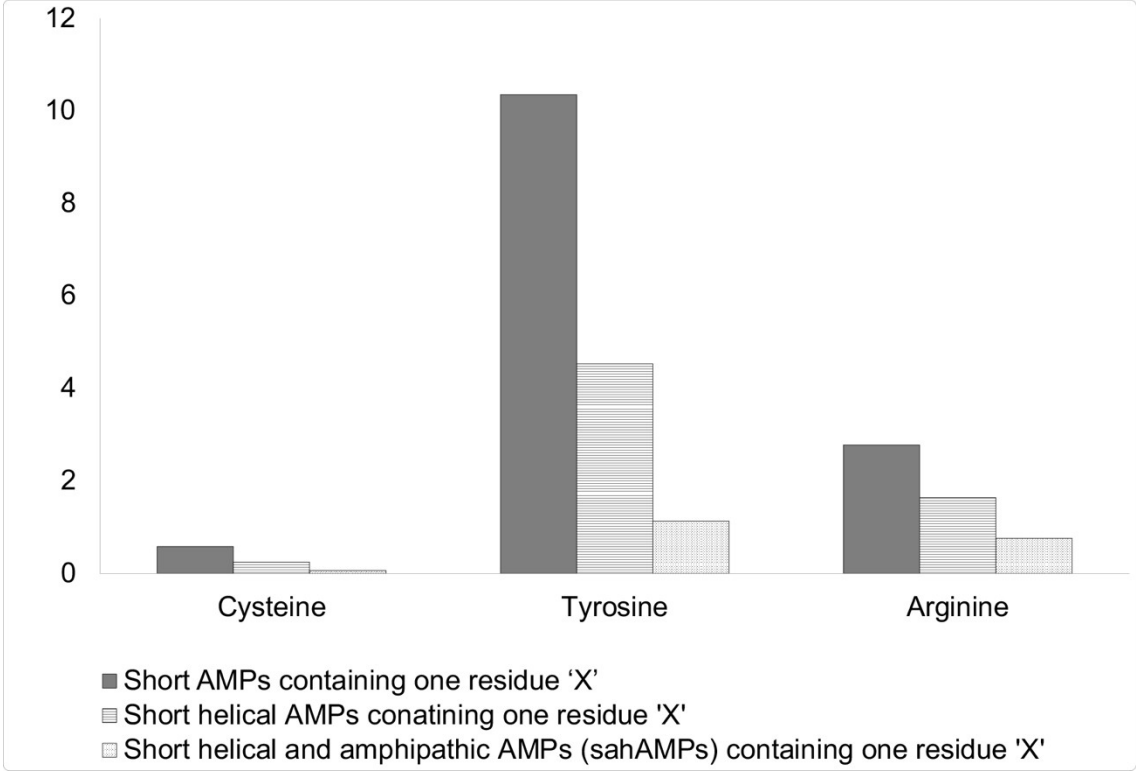

Figure 8. sahAMPs with an odd number or single residues of cysteines are particularly rare. Graphical presentation of the number of AMPs (in three groups) containing a single arginine,

tyrosine, or cysteine, normalized by the frequencies of each residue in AMPs shorter than 40aa. More detailed information is provided in the Experimenal section.

Discussion

AMPs are less likely to induce bacterial resistance compared to conventional small-molecule antibiotics, advocating their therapeutic value. Here, we utilized structural information of the highly stable helical fibril of hLL-$37_{17\text{-}29}$ and explored a means of chemically-controlled regulation of AMPs assembly into functional supramolecular structures. The tunability of intermolecular disulfide bonds mediated activity is shown here for hLL-$37_{17\text{-}29}$, and was further demonstrated with amphibian uperin 3.5, which forms supramolecular helical fibrils as well[47].

DTT abolished activity of all cysteine mutants of hLL-$37_{17\text{-}29}$ against at least one bacterial species (Figure 3), indicating their disulfide-dependent specific bacteriostatic activity. Yet, the extent of the effect of DTT was dependent on the location of the cysteine substitution within the amphipathic helix. The most prominent effect was on the I24C, F17C, I20C, V21C and L28C mutants, which all bear substitutions on the hydrophobic face of the amphipathic helix (Figure 3 and Table S3b), where reduction of the disulfide bond potentially destabilizes the formed supramolecular structure. Theoretically, it is possible that a disulfide bond connecting the hydrophobic faces of sahAMPs would expose hydrophilic surfaces that would deter further amorphous aggregation, and yet, might promote ordered structures with specific inter-helical polar interactions, as was shown here by the atomic structure of the hLL-$37_{17\text{-}29}$ I24C mutant.

The position of Ile24 is located right at the foci of the hydrophobic moment vector of the hLL-$37_{17\text{-}29}$ amphipathic helix (Figure 3 and Table S3b), and in the most buried core of the four-helix bundle of the hLL-$37_{17\text{-}29}$ fibril[21] (Table S2). In accordance with its critical structural location, substitutions of Ile24 to polar residues indeed abolished its bacteriostatic activity against *M.*

luteus[21]. Even a milder substitution to alanine, which is more hydrophobic than cysteine, but still less hydrophobic than isoleucine[72], abolished bacteriostatic activity against *M. luteus* and the formation of ordered fibrils of hLL-$37_{17\text{-}29}$[21]. It was therefore predicted that the activity of I24C, if any, will be dependent on the formation of disulfide bond-mediated assembly. The I24C mutant was not active against *S. hominis*, *E. coli* and *P. fluorescens.* It remained active against *M. luteus*, but only under oxidizing conditions, which support the formation of a disulfide bond and assembly of supramolecular fibrils, as shown by the crystal structure. Reducing conditions indeed dissembled the ordered assembly of the I24C mutant, as demonstrated by the marked shift in particle size distribution towards small particles (Figure 4 and Table S4), and as visualized in Figure 5. The I24C mutant is inactive against *S. hominis* and consistently, there are no observed ordered structures around *S. hominis* cells with or without DTT (Figure 6).The results further support the important role of self-assembly in hLL-$37_{17\text{-}29}$ antibiotic activity[21], as well as the effect of specific cell membranes on peptide assembly.

DTT was least effective in altering the activity of the mutants bearing K18C and Q22C substitutions, which are located on the polar face of the helix (Figure 3 and Table S3). Theoretically, a disulfide bond connecting the polar face of the helix could hinder the formation of ordered fibrillar structures featuring a hydrophobic core. Therefore, one conjecture is that the K18C and Q22C mutants are active, to the same extent, as monomers, covalent dimers, or as amorphous aggregate. Yet a more plausible hypothesis is that these mutants self-assemble regardless of the formation of a disulfide bond. This may be possible via an extensive fibrillar hydrophobic core featuring a more extensive surface area buried along with a network of interactions, as shown for hLL-$37_{17\text{-}29}$[21] and its I24C mutant (Figures 1-2 and Figures S1&S3), compared to an isolated covalent dimer. In accordance with this hypothesis, while DTT had a

significant effect on I24C activity, it had no effect on Q22C particle size distribution, which remained primarily composed of large particles (Figure 4 and Table S4). As observed for the I24C mutant, which does not form aggregates in the presence of *S. hominis* in contrast to around *M. luteus* cells, the morphology of the aggregate and mechanism of action might be dependent on the specific bacteria. Specifically, DTT abolished the activity of the K18C mutant against *E. coli*, and of the Q22C mutant against *S. hominis*, but not against other species (Figure 3). Electron micrographs indeed showed that while Q22C formed massive aggregates around *S. hominis* cells, the morphology was very different in the presence of DTT (Figure 6), supporting a morphology-dependent activity.

Both crystal structures of hLL-$37_{17\text{-}29}$ and its I24C mutant, although different, were associated with fibrillary structures, with a surface composed of zigzagged hydrophobic and positively charged belts, which likely disrupt bacterial membranes comprised of negatively charged lipid bilayers. DTT had different effects on peptide bacteriostatic activity, depending on the tested mutant and bacterial species, which might be indicative of diverse mechanisms of hLL-$37_{17\text{-}29}$ mutant action against different bacteria. Moreover, the bacterial membranes and cell walls might differentially affect aggregation and fibril morphology, thereby altering toxicity level. Bi-directional effects between membrane lipids and fibril-forming toxins have been previously suggested for the bacterial PSMα3 cytotoxin and the amphibian uperin 3.5 AMP which form helical cross-α amyloid fibrils[47, 73, 74].

To conclude, we demonstrated the correlation between the self-assembly to bacteriostatic activity in fibril-forming sahAMPs. By single point cysteine mutations, they can be deactivated under reducing conditions, but remain active under oxidative conditions, such as in areas of inflammation and cancer cells [30-32, 75]. Since AMP self-assembly can often bear functional

relevance and enhance antimicrobial activity[40], it is possible that the observed selection against sahAMPs with a single or an odd number of cysteine residues (Figure 8) is due to the microorganisms' ability to express reducing factors[32-34]. Another explanation to this negative selection could be that the intermolecular disulfide bonds lead to a reduction in the number of conformational states, and to reduced entropy, similarly to disulfide-mediated protein folding[76-81], and thereby hindering peptide aggregation. The demonstrated control over AMP activity is enabled via regulation of its self-assembly into functional supramolecular structures, which can be used as scaffolds for a wide range of bio and nanotechnology, regenerative medicine and bioengineering applications[82], with the invaluable advantage of an inherent antibacterial activity.

Conclusions

In this work, we demonstrate redox-switchable AMP activity, mediated by regulation of intermolecular disulfide bonds and their central role in the formation of supramolecular structures. For that, we utilized structural and functional information on the active core (residues 17-29) of the human antibacterial and immunomodulatory peptide LL-37[21]. A crystal structure of an LL-37_{17-29} cysteine mutant in a critical position within the fibril supported the formation of disulfide-mediated self-assembly, and the suggested mechanism of action of the fibril, mediated via hydrophobic and positively charged zigzagged belts on its surface that likely interact and damage the bacterial membrane. Further cysteine mutations showed position-dependent activity and specificity against different bacterial strains. The findings indicated the significant functional role of supramolecular assembly and its potential switchability based on environmental conditions. Owing to the observed unique effects of intermolecular disulfide bonds on AMPs' structure, activity, specificity, and regulation, we analyzed and found that single and an odd number of cysteines in short helical and amphipathic AMPs are particularly rare. We speculate

that inter-molecular disulfide bonds have been selected against due to their sensitivity to secretion of reducing factors by microorganisms, as well as to their critical effects on peptide self-assembly. Our findings can advance the design of novel antimicrobials that can be deployed as scaffolds in a wide range of applications in bio- and nanotechnology, regenerative medicine, and bioengineering.

ASSOCIATED CONTENT

Supporting Information. Crystal atomic structure, bacteria growth graphs, crystal atomic structure table, SASA table, sequences and properties of mutant peptides tables, helical wheel, DLS table, MIC table, frequencies of residues table, sequences of AMPs with single cysteine residue table. The following files are available free of charge. (PDF).

AUTHOR INFORMATION

Corresponding Author

* Corresponding author: Meytal Landau - Department of Biology, Technion-Israel Institute of Technology, Haifa 3200003, Israel, and European Molecular Biology Laboratory (EMBL), Hamburg 22607, Germany; https://orcid.org/0000-0002-1743-3430; Email: mlandau@technion.ac.il

Authors

Yizhaq Engelberg - Department of Biology, Technion-Israel Institute of Technology, Haifa 3200003, Israel, https://orcid.org/0000-0001-8104-095X; Email: engelberg@campus.technion.ac.il

Peleg Ragonis-Bachar - Department of Biology, Technion-Israel Institute of Technology, Haifa 3200003, Israel, https://orcid.org/0000-0002-0979-8165; Email: pelegrag@campus.technion.ac.il

Funding Sources

This research was supported by the Israel Science Foundation (grant no. 2111/20), Israel Ministry of Science, Technology & Space (grant no. 3-15517), U.S.-Israel Binational Science Foundation (BSF) (grant no. 2017280), BioStruct-X, funded by FP7, and the iNEXT consortium of Instruct-ERIC.

Notes

The authors declare no competing financial interest.

ACKNOWLEDGMENT

We would like to thank Eilon Barnea for critical comments and Leehen Mashiah for technical support. We acknowledge technical support provided by Yael Pazy-Benhar and Dikla Hiya at the Technion Center for Structural Biology (TCSB). We acknowledge guidance and support from Yaron Kauffmann from the MIKA Electron Microscopy Center of the Department of Material Science & Engineering at the Technion, and from Na’ama Koifman from the Russell Berrie

Electron Microscopy Center of Soft Matter at the Technion, Israel. The synchrotron MX data collection experiments were performed at beamline P14, operated by EMBL Hamburg at the PETRA III storage ring (DESY, Hamburg, Germany). We are grateful to Gleb Bourenkov and the teams at EMBL Hamburg for their assistance.

ABBREVIATIONS

AMPs, antimicrobial peptides, hLL-$37_{17\text{-}29}$, active core peptide of the human AMP LL-37, ROS, reactive oxygen species, sahAMPs, short amphipathic helices, *M. luteus*, *Micrococcus luteus*, *S. hominis*, *Staphylococcus hominis*, *P. fluorescens*, *Pseudomonas fluorescens*, *E. coli*, *Escherichia coli*, LB, Luria-Bertani medium, BHI, brain-heart infusion medium, DLS, dynamic light scattering, TEM, Transmission electron microscopy, MIC, minimal inhibitory concentrations, UPddw Ultra-pure double distilled water,

REFERENCES

(1) Jenssen, H.; Hamill, P.; Hancock, R. E. Peptide antimicrobial agents. *Clin. Microbiol. Rev* **2006**, *19* (3), 491-511. DOI: 10.1128/CMR.00056-05.

(2) Shai, Y. From innate immunity to de-novo designed antimicrobial peptides. *Curr. Pharm. Des* **2002**, *8* (9), 715-725. DOI: 10.2174/1381612023395367.

(3) Mader, J. S.; Hoskin, D. W. Cationic antimicrobial peptides as novel cytotoxic agents for cancer treatment. *Expert Opin. Invest. Drugs* **2006**, *15* (8), 933-946. DOI: 10.1517/13543784.15.8.933.

(4) Lai, Y.; Villaruz, A. E.; Li, M.; Cha, D. J.; Sturdevant, D. E.; Otto, M. The human anionic antimicrobial peptide dermcidin induces proteolytic defence mechanisms in staphylococci. *Mol. Microbiol* **2007**, *63* (2), 497-506. DOI: 10.1111/j.1365-2958.2006.05540.x.

(5) Gonzalez, D. J.; Okumura, C. Y.; Hollands, A.; Kersten, R.; Akong-Moore, K.; Pence, M. A.; Malone, C. L.; Derieux, J.; Moore, B. S.; Horswill, A. R.; et al. Novel phenol-soluble modulin derivatives in community-associated methicillin-resistant Staphylococcus aureus identified through imaging mass spectrometry. *J. Biol. Chem* **2012**, *287* (17), 13889-13898. DOI: 10.1074/jbc.M112.349860.

(6) Wang, G.; Narayana, J. L.; Mishra, B.; Zhang, Y.; Wang, F.; Wang, C.; Zarena, D.; Lushnikova, T.; Wang, X. Design of Antimicrobial Peptides: Progress Made with Human Cathelicidin LL-37. *Adv. Exp. Med. Biol* **2019**, *1117*, 215-240. DOI: 10.1007/978-981-13-3588-4_12.

(7) Fialho, A. M.; Stevens, F. J.; Das Gupta, T. K.; Chakrabarty, A. M. Beyond host-pathogen interactions: microbial defense strategy in the host environment. Curr. Opin. Biotechnol **2007**, *18* (3), 279-286. DOI: 10.1016/j.copbio.2007.04.001.

(8) Epand, R. F.; Wang, G.; Berno, B.; Epand, R. M. Lipid segregation explains selective toxicity of a series of fragments derived from the human cathelicidin LL-37. *Antimicrob. Agents Chemother* **2009**, *53* (9), 3705-3714.DOI: 10.1128/AAC.00321-09.

(9) Schmidtchen, A.; Frick, I. M.; Andersson, E.; Tapper, H.; Bjorck, L. Proteinases of common pathogenic bacteria degrade and inactivate the antibacterial peptide LL-37. *Mol. Microbiol* **2002**, *46* (1), 157-168. DOI: 10.1046/j.1365-2958.2002.03146.x.

(10) Chen, Z.; Yang, G.; Lu, S.; Chen, D.; Fan, S.; Xu, J.; Wu, B.; He, J. Design and antimicrobial activities of LL-37 derivatives inhibiting the formation of Streptococcus mutans biofilm. *Chem. Biol. Drug Des* **2019**, *93.6*, 1175-1185. DOI: 10.1111/cbdd.13419.

(11) Wang, G.; Mishra, B.; Epand, R. F.; Epand, R. M. High-quality 3D structures shine light on antibacterial, anti-biofilm and antiviral activities of human cathelicidin LL-37 and its fragments. *Biochim. Biophys. Acta* **2014**, *1838* (9), 2160-2172. DOI: 10.1016/j.bbamem.2014.01.016.

(12) Johansson, J.; Gudmundsson, G. H.; Rottenberg, M. E.; Berndt, K. D.; Agerberth, B. Conformation-dependent antibacterial activity of the naturally occurring human peptide LL-37. *J. Biol. Chem* **1998**, *273* (6), 3718-3724. DOI: 10.1074/jbc.273.6.3718.

(13) Deplanche, M.; Filho, R. A.; Alekseeva, L.; Ladier, E.; Jardin, J.; Henry, G.; Azevedo, V.; Miyoshi, A.; Beraud, L.; Laurent, F.; et al. Phenol-soluble modulin alpha induces G2/M phase transition delay in eukaryotic HeLa cells. *FASEB J* **2015**, *29* (5), 1950-1959. DOI: 10.1096/fj.14-260513.

(14) Joo, H. S.; Cheung, G. Y.; Otto, M. Antimicrobial activity of community-associated methicillin-resistant Staphylococcus aureus is caused by phenol-soluble modulin derivatives. *J. Biol. Chem.* **2011**, *286* (11), 8933-8940. DOI: 10.1074/jbc.M111.221382

(15) Thwaite, J. E.; Hibbs, S.; Titball, R. W.; Atkins, T. P. Proteolytic degradation of human antimicrobial peptide LL-37 by Bacillus anthracis may contribute to virulence. *Antimicrob. Agents Chemother.* **2006**, *50* (7), 2316-2322. DOI: 10.1128/AAC.01488-05.

(16) Lee, J. U.; Kang, D. I.; Zhu, W. L.; Shin, S. Y.; Hahm, K. S.; Kim, Y. Solution structures and biological functions of the antimicrobial peptide, arenicin-1, and its linear derivative. *Pept. Sci. (Hoboken, NJ, U. S.)* **2007**, *88* (2), 208-216. DOI: 10.1002/bip.20700.

(17) Jang, H.; Arce, F. T.; Mustata, M.; Ramachandran, S.; Capone, R.; Nussinov, R.; Lal, R. Antimicrobial protegrin-1 forms amyloid-like fibrils with rapid kinetics suggesting a functional link. *Biophys. J.* **2011**, *100* (7), 1775-1783. DOI: 10.1016/j.bpj.2011.01.072

(18) Zhao, H.; Sood, R.; Jutila, A.; Bose, S.; Fimland, G.; Nissen-Meyer, J.; Kinnunen, P. K. Interaction of the antimicrobial peptide pheromone Plantaricin A with model membranes: implications for a novel mechanism of action. *Biochim. Biophys. Acta, Biomembr.* **2006**, *1758* (9), 1461-1474. DOI: 10.1016/j.bbamem.2006.03.037

(19) Auvynet, C.; El Amri, C.; Lacombe, C.; Bruston, F.; Bourdais, J.; Nicolas, P.; Rosenstein, Y. Structural requirements for antimicrobial versus chemoattractant activities for dermaseptin S9. *FEBS J.* **2008**, *275* (16), 4134-4151. DOI: 10.1111/j.1742-4658.2008.06554.x.

(20) Domanov, Y. A.; Kinnunen, P. K. Antimicrobial peptides temporins B and L induce formation of tubular lipid protrusions from supported phospholipid bilayers. *Biophys. J.* **2006**, *91* (12), 4427-4439. DOI: 10.1529/biophysj.106.091702.

(21) Engelberg, Y.; Landau, M. The Human LL-37(17-29) antimicrobial peptide reveals a functional supramolecular structure. *Nat. Commu.* **2020**, *11* (1), 3894. DOI: 10.1038/s41467-020-17736-x.

(22) Sarkar, T.; Chetia, M.; Chatterjee, S. Antimicrobial Peptides and Proteins: From Nature's Reservoir to the Laboratory and Beyond. *Front. Chem. (Cleveland)* **2021**, *9*, 691532. DOI: 10.3389/fchem.2021.691532.

(23) Simonson, A. W.; Aronson, M. R.; Medina, S. H. Supramolecular Peptide Assemblies as Antimicrobial Scaffolds. *Molecules* **2020**, *25* (12), 2751. DOI: 10.3390/molecules25122751.

(24) Dimarcq, J. L.; Bulet, P.; Hetru, C.; Hoffmann, J. Cysteine-rich antimicrobial peptides in invertebrates. *Pept. Sci. (Hoboken, NJ, U. S.)* **1998**, *47* (6), 465-477. DOI: 10.1002/(SICI)1097-0282(1998)47:6<465::AID-BIP5>3.0.CO;2-#.

(25) Boman, H. G. Peptide antibiotics and their role in innate immunity. *Annu. Rev. Immunol.* **1995**, *13*, 61-92. DOI: 10.1146/annurev.iy.13.040195.000425.

(26) Gerdol, M.; De Moro, G.; Manfrin, C.; Venier, P.; Pallavicini, A. Big defensins and mytimacins, new AMP families of the Mediterranean mussel Mytilus galloprovincialis. *Dev. Comp. Immuno.l* **2012**, *36* (2), 390-399. DOI: 10.1016/j.dci.2011.08.003.

(27) Harris, P. W.; Yang, S. H.; Molina, A.; López, G.; Middleditch, M.; Brimble, M. A. Plant antimicrobial peptides snakin-1 and snakin-2: chemical synthesis and insights into the disulfide connectivity. *Chemistry* **2014**, *20* (17), 5102-5110. DOI: 10.1002/chem.201303207

(28) Fahrner, R. L.; Dieckmann, T.; Harwig, S. S.; Lehrer, R. I.; Eisenberg, D.; Feigon, J. Solution structure of protegrin-1, a broad-spectrum antimicrobial peptide from porcine leukocytes. *Chem. Biol. (Oxford, U. K.)* **1996**, *3* (7), 543-550. DOI: 10.1016/S1074-5521(96)90145-3.

(29) Park, C. H.; Valore, E. V.; Waring, A. J.; Ganz, T. Hepcidin, a urinary antimicrobial peptide synthesized in the liver. *J. Biol. Chem.* **2001**, *276* (11), 7806-7810. DOI: 10.1074/jbc.M008922200.

(30) Scott, M. G.; Davidson, D. J.; Gold, M. R.; Bowdish, D.; Hancock, R. E. The human antimicrobial peptide LL-37 is a multifunctional modulator of innate immune responses. *J. Immunol.* **2002**, *169* (7), 3883-3891.DOI: 10.4049/jimmunol.169.7.3883.

(31) Fang, F. C. Antimicrobial actions of reactive oxygen species. *mBio* **2011**, *2* (5), e00141-11. DOI: 10.1128/mBio.00141-11.

(32) Reniere, M. L. Reduce, induce, thrive: bacterial redox sensing during pathogenesis. *J. Bacteriol.* **2018**, *200* (17), e00128-18. DOI: JB.00128-18

(33) Mu, K.; Wang, D.; Kitts, D. D. Molecular mechanisms that define redox balance function in pathogen-host interactions—is there a role for dietary bioactive polyphenols? *Int. J. Mol. Sci.* **2019**, *20* (24), 6222. DOI: 10.3390/ijms20246222.

(34) Paiva, C. N.; Bozza, M. T. Are reactive oxygen species always detrimental to pathogens? *Antioxid. Redox Signaling* **2014**, *20* (6), 1000-1037. DOI: 10.1089/ars.2013.5447.

(35) Schroeder, B. O.; Wu, Z.; Nuding, S.; Groscurth, S.; Marcinowski, M.; Beisner, J.; Buchner, J.; Schaller, M.; Stange, E. F.; Wehkamp, J. Reduction of disulphide bonds unmasks potent antimicrobial activity of human beta-defensin 1. *Nature* **2011**, *469* (7330), 419-423. DOI: 10.1038/nature09674.

(36) Brzoza, P.; Godlewska, U.; Borek, A.; Morytko, A.; Zegar, A.; Kwiecinska, P.; Zabel, B. A.; Osyczka, A.; Kwitniewski, M.; Cichy, J. Redox Active Antimicrobial Peptides in Controlling

Growth of Microorganisms at Body Barriers. *Antioxidants* **2021**, *10* (3), 446. DOI: ARTN 44610.3390/antiox10030446.

(37) Wehkamp, J.; Salzman, N. H.; Porter, E.; Nuding, S.; Weichenthal, M.; Petras, R. E.; Shen, B.; Schaeffeler, E.; Schwab, M.; Linzmeier, R.; et al. Reduced Paneth cell alpha-defensins in ileal Crohn's disease. *Proc. Natl. Acad. Sci. U. S. A.* **2005**, *102* (50), 18129-18134. DOI: 10.1073/pnas.0505256102.

(38) Karim, C. B.; Paterlini, M. G.; Reddy, L. G.; Hunter, G. W.; Barany, G.; Thomas, D. D. Role of cysteine residues in structural stability and function of a transmembrane helix bundle. *J. Biol. Chem.* **2001**, *276* (42), 38814-38819. DOI: 10.1074/jbc.M104006200.

(39) Bladon, C. M.; Bladon, P.; Parkinson, J. A. Delta-toxin and analogues as peptide models for protein ion channels. *Biochem. Soc. Trans.* **1992**, *20* (4), 862-864. DOI: 10.1042/bst0200862.

(40) Malekkhaiat Häffner, S.; Malmsten, M. Influence of self-assembly on the performance of antimicrobial peptides. *Curr. Opin. Colloid Interface Sci.* **2018**, *38*, 56-79. DOI: https://doi.org/10.1016/j.cocis.2018.09.002.

(41) Tian, X.; Sun, F.; Zhou, X. R.; Luo, S. Z.; Chen, L. Role of peptide self-assembly in antimicrobial peptides. *J. Pept. Sci.* **2015**, *21* (7), 530-539. DOI: 10.1002/psc.2788.

(42) Haffner, S. M.; Malmsten, M. Influence of self-assembly on the performance of antimicrobial peptides. *Curr. Opin. Colloid Interface Sci.* **2018**, *38*, 56-79. DOI: 10.1016/j.cocis.2018.09.002.

(43) Lombardi, L.; Shi, Y. J.; Falanga, A.; Galdiero, E.; de Alteriis, E.; Franci, G.; Chourpa, I.; Azevedo, H. S.; Galdiero, S. Enhancing the Potency of Antimicrobial Peptides through

Molecular Engineering and Self-Assembly. *Biomacromolecules* **2019**, *20* (3), 1362-1374. DOI: 10.1021/acs.biomac.8b01740.

(44) Lee, E. Y.; Zhang, C. S.; Di Domizio, J.; Jin, F.; Connell, W.; Hung, M.; Malkoff, N.; Veksler, V.; Gilliet, M.; Ren, P. Y.; et al. Helical antimicrobial peptides assemble into protofibril scaffolds that present ordered dsDNA to TLR9. *Nat. Commun.* **2019**, *10*, 1-10. DOI: ARTN 101210.1038/s41467-019-08868-w.

(45) Leithold, L. H.; Jiang, N.; Post, J.; Ziehm, T.; Schartmann, E.; Kutzsche, J.; Shah, N. J.; Breitkreutz, J.; Langen, K. J.; Willuweit, A.; et al. Pharmacokinetic Properties of a Novel D-Peptide Developed to be Therapeutically Active Against Toxic beta-Amyloid Oligomers. *Pharm. Res.* **2016**, *33* (2), 328-336. DOI: 10.1007/s11095-015-1791-2.

(46) Wei, G.; Su, Z.; Reynolds, N. P.; Arosio, P.; Hamley, I. W.; Gazit, E.; Mezzenga, R. Self-assembling peptide and protein amyloids: from structure to tailored function in nanotechnology. *Chem. Soc. Rev.* **2017**, *46* (15), 4661-4708, DOI: 10.1039/C6CS00542J.

(47) Salinas, N.; Tayeb-Fligelman, E.; Sammito, M. D.; Bloch, D.; Jelinek, R.; Noy, D.; Usón, I.; Landau, M. The amphibian antimicrobial peptide uperin 3.5 is a cross-α/cross-β chameleon functional amyloid. *Proc. Natl. Acad. Sci. U. S. A.* **2021**, *118* (3), e2014442118. DOI: 10.1073/pnas.2014442118.

(48) Donnarumma, G.; Buommino, E.; Fusco, A.; Paoletti, I.; Auricchio, L.; Tufano, M. A. Effect of temperature on the shift of Pseudomonas fluorescens from an environmental microorganism to a potential human pathogen. *Int. J. Immunopathol. Pharmacol.* **2010**, *23* (1), 227-234. DOI: 10.1177/039463201002300120.

(49) Rainey, P. B. Adaptation of Pseudomonas fluorescens to the plant rhizosphere. *Environ. Microbiol* **1999**, *1* (3), 243-257. DOI: 10.1046/j.1462-2920.1999.00040.x.

(50) Kabsch, W. XDS. *Acta Crystallogr., Sect. D: Biol. Crystallogr.* **2010**, *66* (Pt 2), 125-132. DOI: 10.1107/s0907444909047337.

(51) McCoy, A. J.; Grosse-Kunstleve, R. W.; Adams, P. D.; Winn, M. D.; Storoni, L. C.; Read, R. J. Phaser crystallographic software. *J. Appl. Crystallogr.* **2007**, *40* (4), 658-674. DOI: 10.1107/S0021889807021206.

(52) Winn, M. D.; Ballard, C. C.; Cowtan, K. D.; Dodson, E. J.; Emsley, P.; Evans, P. R.; Keegan, R. M.; Krissinel, E. B.; Leslie, A. G.; McCoy, A.; et al. Overview of the CCP4 suite and current developments. *Acta Crystallogr., Sect. D: Biol. Crystallogr.* **2011**, *67* (Pt 4), 235-242. DOI: 10.1107/s0907444910045749.

(53) Emsley, P.; Cowtan, K. Coot: model-building tools for molecular graphics. *Acta Crystallogr., Sect. D: Biol. Crystallogr.* **2004**, *60* (Pt 12 Pt 1), 2126-2132. DOI: 10.1107/S0907444904019158.

(54) Pettersen, E. F.; Goddard, T. D.; Huang, C. C.; Couch, G. S.; Greenblatt, D. M.; Meng, E. C.; Ferrin, T. E. UCSF Chimera--a visualization system for exploratory research and analysis. *J. Comput. Chem.* **2004**, *25* (13), 1605-1612. DOI: 10.1002/jcc.20084.

(55) Kyte, J.; Doolittle, R. F. A simple method for displaying the hydropathic character of a protein. *J. Mol. Biol.* **1982**, *157* (1), 105-132. DOI: 10.1016/0022-2836(82)90515-0.

(56) Jurrus, E.; Engel, D.; Star, K.; Monson, K.; Brandi, J.; Felberg, L. E.; Brookes, D. H.; Wilson, L.; Chen, J.; Liles, K.; et al. Improvements to the APBS biomolecular solvation software suite. *Protein Science* **2018**, *27* (1), 112-128. DOI: 10.1002/pro.3280 (acccessed 2020/01/27).

(57) Gautier, R.; Douguet, D.; Antonny, B.; Drin, G. HELIQUEST: a web server to screen sequences with specific alpha-helical properties. *Bioinformatics* **2008**, *24* (18), 2101-2102. DOI: 10.1093/bioinformatics/btn392.

(58) Saff, E. B.; Kuijlaars, A. B. J. Distributing many points on a sphere. *Mathematical Intelligencer* **1997**, *19*, 5-11.

(59) Lee, B.; Richards, F. M. The interpretation of protein structures: estimation of static accessibility. *J. Mol. Biol* **1971**, *55* (3), 379-400. DOI: 10.1016/0022-2836(71)90324-X.

(60) Consortium, U. Update on activities at the Universal Protein Resource (UniProt) in 2013. *Nucleic Acids Res.* **2013**, *41* (Database issue), D43-47. DOI: 10.1093/nar/gks1068.

(61) Waghu, F. H.; Barai, R. S.; Gurung, P.; Idicula-Thomas, S. CAMPR3: a database on sequences, structures and signatures of antimicrobial peptides. *Nucleic Acids Res.* **2016**, *44* (D1), D1094-1097. DOI: 10.1093/nar/gkv1051.

(62) Drozdetskiy, A.; Cole, C.; Procter, J.; Barton, G. J. JPred4: a protein secondary structure prediction server. *Nucleic Acids Res.* **2015**, *43* (W1), W389-394. DOI: 10.1093/nar/gkv332.

(63) Fauchere, J. V. P. Hydrophobic parameters II of amino acid side-chains from the partitioning of N-acetyl-amino acid amides. *Eur. J. Med. Chem.* **1983**, *18*, 4.

(64) Eisenberg, D.; Weiss, R. M.; Terwilliger, T. C. The helical hydrophobic moment: a measure of the amphiphilicity of a helix. *Nature* **1982**, *299* (5881), 371-374. DOI: 10.1038/299371a0.

(65) Chou, P.; Fasman, G. D. Amino acid sequence. *Adv. Enzymol. Relat. Areas Mol. Biol.* **2009**, *47*, 45-55.

(66) Sancho-Vaello, E.; Francois, P.; Bonetti, E. J.; Lilie, H.; Finger, S.; Gil-Ortiz, F.; Gil-Carton, D.; Zeth, K. Structural remodeling and oligomerization of human cathelicidin on membranes suggest fibril-like structures as active species. *Sci. Rep.* **2017**, *7* (1), 15371. DOI: 10.1038/s41598-017-14206-1.

(67) Colletier, J.-P.; Laganowsky, A.; Landau, M.; Zhao, M.; Soriaga, A. B.; Goldschmidt, L.; Flot, D.; Cascio, D.; Sawaya, M. R.; Eisenberg, D. Molecular basis for amyloid-beta polymorphism. *Proc. Natl. Acad. Sci. U. S. A.* **2011**, *108* (41), 16938-16943. DOI: 10.1073/pnas.1112600108.

(68) Wiltzius, J. J.; Sievers, S. A.; Sawaya, M. R.; Eisenberg, D. Atomic structures of IAPP (amylin) fusions suggest a mechanism for fibrillation and the role of insulin in the process. *Protein Science* **2009**, *18* (7), 1521-1530. DOI: 10.1002/pro.145.

(69) Close, W.; Neumann, M.; Schmidt, A.; Hora, M.; Annamalai, K.; Schmidt, M.; Reif, B.; Schmidt, V.; Grigorieff, N.; Fandrich, M. Physical basis of amyloid fibril polymorphism. *Nat. Commun.* **2018**, *9* (1), 699. DOI: 10.1038/s41467-018-03164-5.

(70) Tayeb-Fligelman, E.; Tabachnikov, O.; Moshe, A.; Goldshmidt-Tran, O.; Sawaya, M. R.; Coquelle, N.; Colletier, J. P.; Landau, M. The cytotoxic Staphylococcus aureus PSMalpha3

reveals a cross-alpha amyloid-like fibril. *Science* **2017**, *355* (6327), 831-833. DOI: 10.1126/science.aaf4901.

(71) Kumar, T. A. CFSSP: Chou and Fasman secondary structure prediction server. *Wide Spectrum* **2013**, *1* (9), 15-19. DOI: 10.5281/zenodo.50733

(72) Diederichs, K.; Karplus, P. A. Improved R-factors for diffraction data analysis in macromolecular crystallography. *Nat. Struct. Biol.* **1997**, *4* (4), 269-275. DOI: 10.1038/nsb0497-269.

(73) Tayeb-Fligelman, E.; Salinas, N.; Tabachnikov, O.; Landau, M. Staphylococcus aureus PSMalpha3 Cross-alpha Fibril Polymorphism and Determinants of Cytotoxicity. *Structure* **2020**, *28* (3), 301-313.e306. DOI: 10.1016/j.str.2019.12.006

(74) Martin, L. L.; Kubeil, C.; Piantavigna, S.; Tikkoo, T.; Gray, N. P.; John, T.; Calabrese, A. N.; Liu, Y.; Hong, Y.; Hossain, M. A.; et al. Amyloid aggregation and membrane activity of the antimicrobial peptide uperin 3.5. *Pept. Sci. (Hoboken, NJ, U. S.)* **2018**, *110* (3), e24052. DOI: 10.1002/pep2.24052.

(75) Shai, Y. Mode of action of membrane active antimicrobial peptides. *Biopolymers* **2002**, *66* (4), 236-248. DOI: 10.1002/bip.10260.

(76) Murphy, K. P.; Freire, E. Thermodynamics of structural stability and cooperative folding behavior in proteins. *Adv. Protein Chem.* **1992**, *43*, 313-361. DOI: 10.1016/s0065-3233(08)60556-2.

(77) Jensen, K. S.; Hansen, R. E.; Winther, J. R. Kinetic and thermodynamic aspects of cellular thiol-disulfide redox regulation. *Antioxid. Redox Signaling* **2009**, *11* (5), 1047-1058. DOI: 10.1089/ARS.2008.2297.

(78) Peng, L.; Qian, H.; Hong, L. Thermodynamics of Markov processes with nonextensive entropy and free energy. *Phys. Rev. E* **2020**, *101* (2-1), 022114. DOI: 10.1103/PhysRevE.101.022114.

(79) Brady, G. P.; Sharp, K. A. Entropy in protein folding and in protein-protein interactions. Curr. Opin. Struct. Biol. **1997**, *7* (2), 215-221. DOI: 10.1016/s0959-440x(97)80028-0.

(80) Betz, S. F. Disulfide bonds and the stability of globular proteins. *Protein Science* **1993**, *2* (10), 1551-1558. DOI: 10.1002/pro.5560021002.

(81) Harrison, P. M.; Sternberg, M. J. Analysis and classification of disulphide connectivity in proteins. The entropic effect of cross-linkage. *J. Mol. Biol.* **1994**, *244* (4), 448-463. DOI: 10.1006/jmbi.1994.1742.

(82) Hughes, S. A.; Wang, F.; Wang, S.; Kreutzberger, M. A. B.; Osinski, T.; Orlova, A.; Wall, J. S.; Zuo, X.; Egelman, E. H.; Conticello, V. P. Ambidextrous helical nanotubes from self-assembly of designed helical hairpin motifs. *Proc. Natl. Acad. Sci. U. S. A.* **2019**, *116* (29), 14456-14464. DOI: 10.1073/pnas.1903910116.

For Table of Contents Use Only